Smart Structures and Systems, *Vol. 23, No. 4 (2019) 347-357*
DOI: https://doi.org/10.12989/sss.2019.23.4.347

Application of dithering control for the railway wheel squealing noise mitigation

Seyed Rahim Marjani[a] and Davood Younesian*

School of Railway Engineering, Iran University of Science and Technology, Tehran 16846-13114, Iran

(Received August 11, 2018, Revised February 22, 2019, Accepted February 27, 2019)

Abstract. A new methodology for mitigation of the wheel squealing is proposed and investigated based on the dithering control. The idea can be applied in railway lines particularly in urban areas. The idea is clearly presented, and applied to a validated model. A full-scale model including the vehicle, curved track and wheel/rail contact is developed in the time domain to analyze the possibility and level of wheel squeal noise. Comparing the numerical results with a field test, the model is validated in different levels namely i) occurrence, ii) squealing frequency and iii) noise level. Two different approaches are proposed a) dithering of the wheel with piezoelectric patches and b) dithering of the rail with piezoelectric stacks. The noise level as well as the wheel responses is compared after applying the control strategy. A parametric study is carried out and effect of the dithering voltage and frequency on the squealing noise is investigated. It is found that both the strategies perform quite effectively within the saturating threshold of piezoelectric actuators.

Keywords: squealing; wheel; control; piezoelectric; dithering

1. Introduction

The wheel squeal is usually known as a monotonic, high frequency and high level railway noise. Cause of the wheel squeal is a typical self-excited vibration of the wheel due to stick-slip in the contact patch as result of negative slope of the friction-creepage relation on high creepage. It normally happens when the train passes sharp curves and lateral creepage of wheel on rail gets more than critical creepage. Stick-slip in a multi-degree of freedom self-excited vibrating system has been modeled and analyzed by Ranjbar and Tadayon (2017).

It has been reported that curve squeal is the dominate source of train noise at frequencies above 125 Hz Soeta and Shimokura (2013). North railway has one of oldest lines in Iran. Due to passing through mountain areas, there are several tight curves with less than 300 m radius along this line. The noise of traveling trains has brought nowadays discomfort and complains to the adjacent residents. Reports show that one of the main sources is the wheel squealing recognized by its tonal spectrum. The purpose of this study is finding a semi-active and effective solution for reducing squealing noise applicable in similar lines.

Noise measurement is one of the most common primary steps for studying the wheel squeal. Different methods have been applied so far to the wheel squeal noise measurement. They can be categorized based on the measurement variables and sensors placement. The wheel noise might be measured and analyzed by installing the microphones on the bogie, close to the wheel (Vincent *et al*. 2006) or locating microphones next to the railway track (Stefanelli *et al.* 2006, Volz and Feldman 2007, Anderson *et al.* 2008, Glocker *et al.* 2009, Meehan *et al.* 2010, Hanson *et al*. 2014). The first method is more efficient to precisely identify the wheel squeal source but it is more expensive and complicated. The other method is usually more suitable to study environmental aspects of the squeal noise in neighborhood of the railway tracks. Unstable vibration inner wheel of the bogie's front axle is introduced as the main source of squeal noise according to previous studies. Frequency analysis of the measured noise shows that axial vibration mode shapes are dominant in squeal noise spectrum. Effects of different parameters such as the attack angle (Anderson *et al.* 2008), train speed (Meehan *et al.* 2010), rail parameters (Volz and Feldman 2007, Hanson *et al.* 2014) and humidity (Meehan *et al.* 2010) have been investigated by different researchers. According to the presented results, the rail is not an effective source of squeal noise and the attack angle, train velocity and humidity influence the squeal noise level and occurrence but not its frequency.

Different models have been presented so far in time and frequency domains for simulation and analysis of the wheel squeal. Modeling in frequency domain is normally used for prediction of the wheel squeal occurrence and also for parametric study to the squeal threshold. However, for calculating the vibration and noise level, a time domain model is normally required. An experimentally validated model in frequency domain has been applied for prediction and investigation of wheel squeal in presence of one (Monk-Steel and Thompson 2003, Marjani and Younesian 2017) and two contact points (Squicciarini *et al.* 2015). Those models take the wheel and track dynamics, contact force and rail vehicle dynamics into account.

*Corresponding author, Professor
E-mail: younesian@iust.ac.ir
[a] Ph.D. Student

http://www.techno-press.com/journals/sss&subpage=7 ISSN: 1738-1584 (Print), 1738-1991 (Online)

Huang *et al.* (2007) transferred similar models to the time domain and applied that for the wheel squeal analysis. Pieringer (2014) developed a new precise model for the wheel/rail interaction in high-frequency range to study the curve squeal in constant wheel/rail friction. It was shown that the wheel squeal can occur in the absence of negative slope of the friction. Based on the energy method and result of laboratory tests, Liu and Meehan (2015) presented a simplified model to study the influence of velocity and angle of attack. Shape optimization is always a solution for improvement of acoustic performance in many engineering applications. Ranjbar *et al.* (2010, 2012a, b) examined different optimization techniques and found that the method of moving asymptotes (MMA) is the most appropriate technique for acoustical shape optimization of thin-walled structures. However, due to safety and several other operational limitations we cannot straightforwardly change the wheel profile just because of squealing cancellation.

Researchers suggested various methods for decreasing or canceling of the wheel squeal noise. All methods can be classified into two main groups. In the first category, methods focus on the wheel/rail interaction as the main source of wheel excitation. Rail lubrication (Hanson *et al.* 2014, Curley *et al.* 2017, Garg and Sharma 2010), asymmetric grinding of the rails in curves (Müller and Oertli 2006) and railhead optimization (Hiensch *et al.* 2007) are in this class. Rail lubrication is widely used for reducing the wheel squeal noise but it can cause loss of adhesion and increases the maintenance costs. The two other methods are still under study in different research centers. Purpose of the methods in the second category is to reduce the wheel vibration by increasing its structural damping. Efficiency of the added damping in decreasing the wheel squeal noise has been analytically and experimentally proved. These methods include dynamic vibration absorbers (Shakeri and Younesian 2016, Rusli *et al.* 2015), double metallic damping ring (Brunel *et al.* 2010), inserting preload ring in the wheel rim (Brunel *et al.* 2004), and mounting damping layers (Merideno *et al*. 2014).

In recent years, application of the piezoelectric actuators for active and passive control of vibration is widely studied (Li *et al*. 2014, Zenz *et al.* 2013). Marjani and Younesian (2017) investigated piezoelectric actuators in wheel squealing noise suppression.

But all these methods must be specifically designed for each wheel and there are limitations for any of them. In this study, a novel solution is suggested based on the dither signal induced in the rail or wheel by piezoelectric actuators. Dithering is a high-frequency and very low amplitude excitation that applied on one of bodies that are connected. It can effectually negate the negative slope in the friction-creepage relationship (Thomsen 1999). As result the dither control prevents stick-slip phenomenon in the contact point and has been addressed in other dynamical systems (Lin *et al*. 2015, Teoh and MohdRipin 2017). It will be shown that dither control is effective method for wheel squeal noise suppression.

In this study, noise next to a curved track has been measured and the experimental and field test results are used to validate the model. The steady-state parameters are determined by multi-body dynamics software. Wheel modal data are obtained by the FEA modeling and they are validated by experimental modal test. All these is used for a comprehensive wheel squeal model including wheelset dynamics, track dynamics, nonlinear contact force and train curving dynamics. The model is used for the investigation of dither control by piezoelectric actuators applied to the wheel or rail. The main contribution of this paper is to propose and evaluate performance of a new control strategy based on the dithering. It is shown that dither control is effective in suppression of the wheel squeal noise.

2. Wheel squeal noise measurement

The selected curve is located in the north of Iran in the middle of two villages. The geometry of the curve and is summarized in Table 1. Traffic of this line is mixed type having freight and passenger trains. The noise measurement is performed for both types of trains. The velocity is 45 km/h for freight cars and 60 km/h for passenger cars in this curve. The location of microphones is shown in Fig. 1. Frequency analysis is used for investigation of the recorded noise. In this study, 4 microphones are used which are capable of measuring up to 4 kHz. The height of microphone 1, 3 and 4 is 1.5 m and height of microphone 2 is 0.5 m above the rail head.

2.1 Measurement data analysis

Fig. 2 shows the frequency analysis of the measurement results for passenger and freight trains. As can be seen, the wheel squeal occurred when the freight car passed the curve.

Table 1 curve properties

Radius	Length	Super elevation	Axle load
220 m	800 m	136 mm	20 Ton

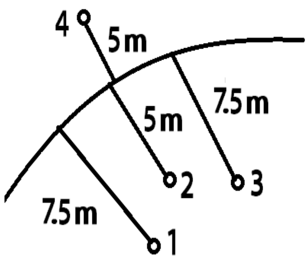

(a)

(b)

Fig. 1 Microphones placement on noise measurement

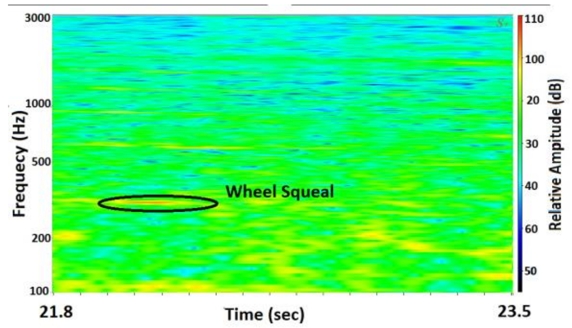

(a) Passenger train

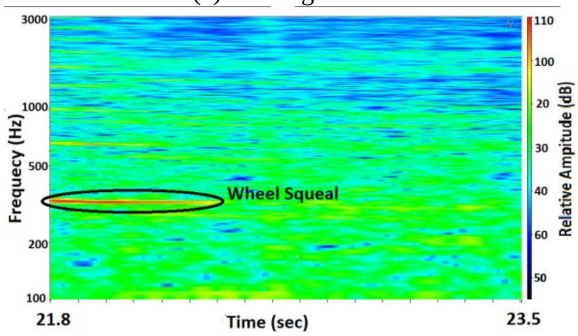

(b) Freight train

Fig. 2 Noise spectrum, microphone

For passenger car, the level of squeal noise is lower. It can be the result of a more flexible suspension and lower attack angle. As seen in Fig. 2, main frequency of the squeal noise is 350 Hz.

3. Transient wheel squeal model

The wheel squeal model is briefly explained in this section. The model includes wheelset dynamics, vertical and lateral track dynamics and nonlinear contact theory and it also takes vehicle dynamics into account. Vibration of the wheelset is solved and it is fed into a calculation package to determine the sound pressure level (SPL) by using the method presented by Younesian *et al.* (2015).

The relationship between different parts of the wheel squeal model is illustrated in Fig. 3. In the first step, simulation begins by a disturbance input.

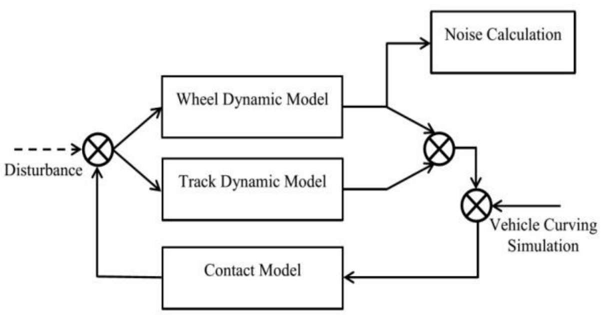

Fig. 3 Transient wheel squeal model

Then the wheel and rail responses are calculated. Wheel lateral response is used for the noise calculations. Contact forces are obtained according to the wheel and rail responses in contact point. The loop repeats by replacement of disturbance by contact force. The transient simulation is fulfilled by the step by step integration.

3.1 Wheelset dynamic model

Wheelset modal data is used for dynamic modeling. Natural frequencies and mode shapes are calculated by FEM software and verified by an experimental modal test. Also modal damping can be estimated based on the Ref. Jones and Thompson (2000) as

$$\eta = \begin{cases} 0.001 & n = 0 \\ 0.01 & n = 1 \\ 0.0001 & n \geq 2 \end{cases} \tag{1}$$

in which, n is the number of nodal diameters. Equation of motion for the wheelset is represented by

$$\dot{\bar{y}}^w = \left[A^w\right]\bar{y}^w + \left[B^w\right]\bar{f}^w \tag{2}$$

$$\bar{v}^w = \left[C^w\right]\bar{y}^w \tag{3}$$

in the state-space, where $\bar{y}_w$ is a 2n-order state-variable vector including modal velocity $\dot{\bar{q}}_r$ and the modal displacement $\bar{q}_r$ for the mode r (1 to n),

$$\bar{y}^w = \{\dot{q}_1, \dot{q}_2, \ldots, \dot{q}_n, q_1, q_2, \ldots, q_n\}^T = \{y_1^w, y_2^w, \ldots, y_{2n}^w\}^T \tag{4}$$

where, $\bar{f}^w = \{f_2^w, f_3^w\}$ and $\bar{v}^w = \{v_2^w, v_3^w\}$ are input dynamic forces and output dynamic velocities in lateral and vertical directions respectively. The system matrix [A^w], the input matrix [B^w] and output matrix [C^w] are obtained by using the modal data in the state space according to Squicciarini *et al*. (2015).

3.2 Track dynamics

Effect of the track response inside the contact point cannot be ignored for contact force calculation. The vertical track dynamic model is based on the Sadeghi *et al.* (2016). The rail is modeled as an infinite Timoshenko beam. Sleepers are assumed to be concentrated mass elements. Discrete linear springs and dampers are used for modeling the pad and ballast.

The rail deformation must be in addition considered to model lateral track dynamics in high frequencies. Therefore, the rail is modeled by three attached beams including two infinite Timoshenko beams for the rail head and foot and another beam for the rail web (Jiang *et al.* 2013, Knothe and Wu 1998, Younesian and Kargarnovin 2009).

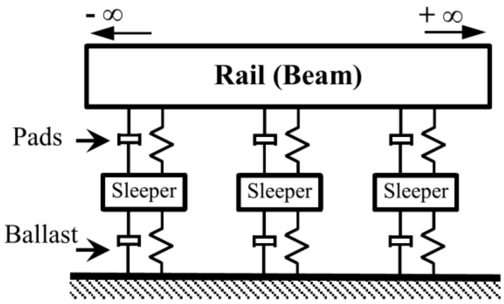

(a) Vertical

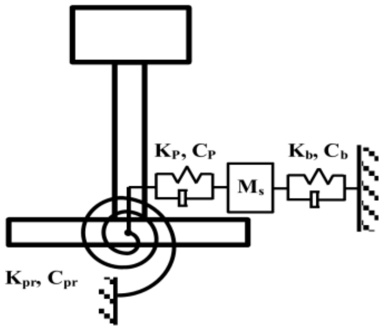

(b) Lateral

Fig. 4 Track model (Jiang *et al*. 2013, Knothe and Wu 1998)

FEA package is used for calculating the track frequency response in both vertical and lateral directions. The track equation of motion in state space can be then represented by

$$\dot{\bar{y}}^r_{2,3} = \left[A^r_{2,3}\right]\bar{y}^r_{2,3} + \left[B^r_{2,3}\right]\bar{f}^r_{2,3} \tag{5}$$

$$\bar{v}^r_{2,3} = \left[C^r_{2,3}\right]\bar{y}^r_{2,3} \tag{6}$$

3.3 Contact theory

Fig. 5 shows the contact coordinate system on the wheel. Perpendicular to the contact patch is taken as direction 3, lateral direction as 2 and direction of motion along track line as 1.

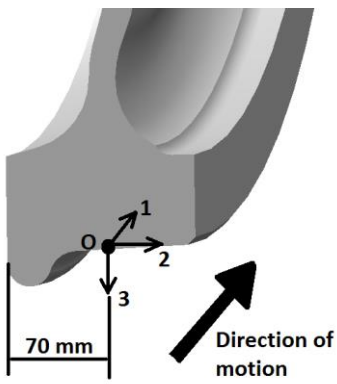

Fig. 5 Coordinate system on right wheel

The vertical force in contact point F_3, can be calculated by Monk-Steel and Thompson (2003)

$$F_3 = N + k_h.\Delta w_3 \tag{7a}$$

$$\Delta w_3 = \left(w^w_3 - w^r_3\right) \tag{7b}$$

where N is the static vertical force on the contact patch that is obtained by vehicle dynamic analysis, k_H is the Hertzian contact spring stiffness; w^w_3 and w^r_3 are the wheel and rail vertical deflections in the contact point.

The lateral force F_2 connects the vertical force to the lateral friction coefficient μ_2

$$F_2 = \mu_2(\gamma_2)F_3 \tag{8}$$

The lateral fiction coefficient is a function of lateral creepage γ_2. Lateral creepage is caused by the lateral displacement of the wheel relative to the rail and is defined by

$$\gamma_2 = \frac{v^r_2 - v^w_2}{V} \tag{9}$$

in which, v^r_2 and v^w_2 are the rail and wheel lateral velocity in contact point and V denotes the train speed. The for modeling lateral friction coefficient Vermeulen-Johnson is used that can be obtained by the following equation Hanson *et al*. (2014),

$$\mu_2 = \left\{\begin{matrix} \mu_0\left(\Gamma_2 - \frac{1}{3}\Gamma_2^{\,2} + \frac{1}{27}\Gamma_2^{\,3}\right) \quad for\ \Gamma_2 < 3 \\ \mu_0 \quad for\ \Gamma_2 > 3 \end{matrix}\right\} \tag{10}$$

where the rolling friction coefficient μ_0 and normalized creepage Γ_2 can be calculated by

$$\mu_0(\gamma_2) = \mu_{stat}\left\{1 - 0.5\mathrm{e}^{-0.138/|\gamma_2 V|} - 0.5\mathrm{e}^{-6.9/|\gamma_2 V|}\right\} \tag{11}$$

$$\Gamma_2 = \frac{GC_{22}ab}{\mu_0 N}\gamma_2 \tag{12}$$

In the above equations a, b are the semi-axis length of the Hertz contact ellipse in the rolling and lateral direction (m), G is the shear modulus of steel and C_{22} the Kalker constant presented in (Kalker 1991, Kouroussis *et al.* 2014). In saturation region, static friction coefficient is calculated by

$$\mu_{stat} = \frac{\tau_R \tau_W}{\tau_R + \tau_W}\frac{\pi ab}{N} \tag{13}$$

where τ_W, τ_R are the shear strength of the wheel and rail material. Fig. 6 shows the general trend of the lateral friction coefficient as a function of the lateral creepage.

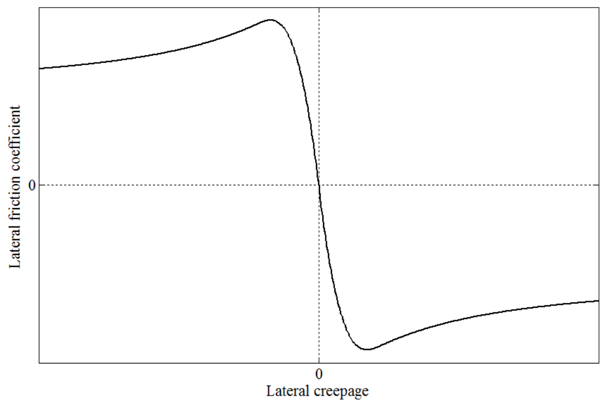

Fig. 6 General form of lateral friction coefficient

3.4 Noise calculation

Vibration profile for the points on outside wheel surface is used for calculating acoustic pressure in desired point P. The wheel surface is meshed into different surface elements and response of point in the middle of each element is taken into account. Transient response for the acoustic pressure can be calculated by Rayleigh integration approach presented by Shakeri and Younesian (2016),

$$p(R,\varphi,\phi,t)=\frac{\rho_0}{2\pi}\int_{A_{wheel}}\frac{1}{R}\ddot{w}_2^{\,w}\left(r,\theta,t-\frac{R}{c_0}\right)dA \quad (14)$$

R is the distance of the point P and the surface element, c_0 and ρ_0 are the sound propagation velocity and density of the air and $\ddot{w}_2^{\,w}$ denotes the wheel lateral acceleration.

4. Dither control

Dithering here is defined as a high frequency vibration that it is induced in the system for prevention of stick-slip. The negative slope of friction-creepage relationship (Fig. 6) can be effectively canceled by dithering (Thomsen 1999). As result self-excited vibration will be prevented and it causes wheel squeal suppression (Lin *et al.* 2015). In this study, dither signal is applied tangential to the friction surface on the wheel or rail. Piezoelectric actuators are used for supplying such signal. This additional input to the system is schematically shown in Fig. 7.

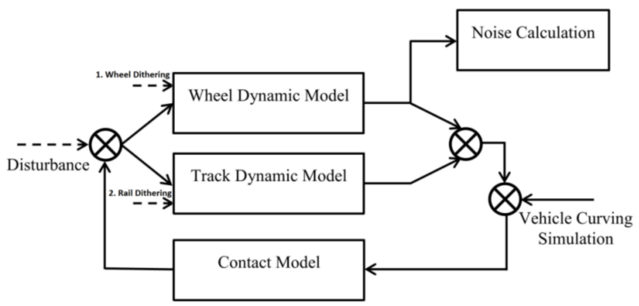

Fig. 7 Transient wheel squeal model in presence of dither signal

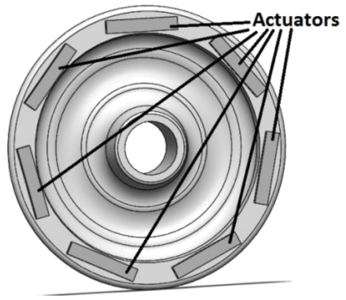

Fig. 8 Piezoelectric patches on the wheel thread

4.1 Dither signal on the wheel

To apply dither signal on the wheel, piezoelectric patches are installed on the wheel thread as shown in Fig. 8. The piezoelectric actuators induce a bending moment and consequent lateral vibration of the wheel on contact surface. The equation of motion of the wheel is presented by

$$\begin{aligned}\dot{\bar{y}}^w &= [A^w]\,\bar{y}^w + [B^w_{actuator}]\,\bar{V}_{actuator} + [B^w]\,\bar{f}^w \\ \bar{v}^w &= \left[C^w\right]\,\bar{y}^w\end{aligned} \quad (15)$$

In the above equations, all matrixes must be reconstructed according to the wheel modal data after attaching piezoelectric actuators. The wheel input matrix of actuator, $B^w_{actuator}$ can be obtained by

$$B^w_{actuator}=K_a\times\left[\begin{array}{cccc|cccc}\phi'^{P11}_{21}-\phi'^{P12}_{21} & \phi'^{P11}_{22}-\phi'^{P12}_{22} & \cdots & \phi'^{P11}_{2n}-\phi'^{P12}_{2n} & 0 & 0 & \cdots & 0\\ \phi'^{P11}_{31}-\phi'^{P12}_{31} & \phi'^{P11}_{32}-\phi'^{P12}_{32} & \cdots & \phi'^{P11}_{3n}-\phi'^{P12}_{3n} & 0 & 0 & \cdots & 0\\ \vdots & \vdots & \ddots & \vdots & \vdots & \vdots & \ddots & \vdots\\ \phi'^{Pm1}_{21}-\phi'^{Pm2}_{21} & \phi'^{Pm1}_{22}-\phi'^{Pm2}_{22} & \cdots & \phi'^{Pm1}_{2n}-\phi'^{Pm2}_{2n} & 0 & 0 & \cdots & 0\\ \phi'^{Pm1}_{31}-\phi'^{Pm2}_{31} & \phi'^{Pm1}_{32}-\phi'^{Pm2}_{32} & \cdots & \phi'^{Pm1}_{3n}-\phi'^{Pm2}_{3n} & 0 & 0 & \cdots & 0\end{array}\right]^T \quad (16)$$

where ϕ'^{Pmi}_{kn} is the wheel mode shape gradient, k is the number of nodal circle , n is the number of nodal diameters and K_a is the actuator coefficient and can be calculated by Kouroussis *et al.* (2014)

$$K_a = b_p\, d_{31}\, E_p (t_p + t_w) \quad (17)$$

where E_p, b_p, t_p and d_{31} respectively denote the Young's modulus, width, thickness and transverse a strain constant of the piezoelectric. t_w is thickness of the wheel in the location of actuator attachment. The voltage of the actuator has sinusoidal form

$$\bar{V}_{actuator} = V_0 \sin\left(\omega_0 t\right) \quad (18)$$

Choosing appropriate voltage amplitude V_0 and voltage frequency ω_0 is important for the suppression of the wheel squeal noise.

4.2 Dither signal on the rail

Piezoelectric stacks are used for applying dither signal on the rail. In this type of actuators, direction of the force and deformation are the same. The actuator installation is shown in Fig. 9. By this configuration, a lateral vibration is induced to the rail tangential to contact surface.

The relation between the applied voltage on piezoelectric actuator ($V_{actuator}$) and the induced force on rail (F_p) is given by

$$F_p = K_A \left(\Delta L - n_p d_{33} V_{actuator} \right) \tag{19}$$

where n_p is the number of piezoelectric, ΔL is the length change of actuator and d_{33} is the strain constant of piezoelectric. K_A denotes the piezoelectric stack constant

$$K_A = \frac{A_p E_p}{L_p} \tag{20}$$

in which, A_p is the area of piezoelectric actuator section. It is assumed that the piezoelectric actuator is fixed in one side and the other side is connected to the rail. Therefore we have

$$F_p = K_A \left(y_2^r - n_p d_{33} V_{actuator} \right) \tag{21}$$

Equation of lateral dynamics of the track is presented by

$$\dot{\bar{r}} = [A_2^r]\ \bar{r} + [B_2^r]\ (f_2^r + F_p) \tag{22}$$

5. Case study

In this study, a similar model to the one in field test measurement is simulated. It consists of a freight wagon with speed of 45 km/h passing through a curve with properties listed in Table 1. Measurement results are used to validate the wheel squeal model.

The first step is to calculate the steady state part of parameters including normal force, stationary lateral creepage, and contact position. Multi-body dynamic software is used for this purpose. The obtained parameters and contact variables are listed in Table 2.

Table 2 Steady state curving parameters

Parameter	Symbol	Unit	Value
Normal force	N	KN	67.8
Stationary lateral creepage	γ_2	---	11.1×10-3

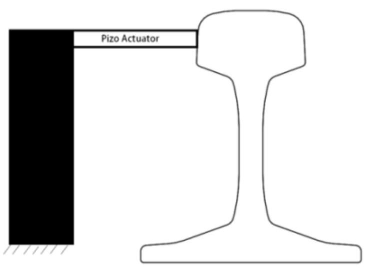

Fig. 9 Installation of the piezoelectric stack on the rail

5.1 Wheel modal characteristics

FEA software is used to calculate the wheel modal data. An experimental modal test is applied for validation of the FEA model. A UIC920 wheelset is taken into consideration with the properties listed in Table 3. Experimental modal analysis with impulse is applied for obtaining the natural frequencies. Fig. 10 shows the modal test setup. For having free-free condition similar to FEM model, the wheelset is placed on a very soft layer. As shown in Fig. 11, three 1-axis accelerometers are used for recording the impulse response. After recording all responses, modal analysis software is used for calculating the natural frequency of the wheelset.

The main axial natural frequencies and mode shapes obtained by FEA and modal test are compared in Table 4. As can be seen, differences between the FEM and the experimental modal results are in an acceptable range.

5.2 Track dynamic model

The track model is based on the standard ballasted track including UIC 60 rail and concrete sleepers spaced 60 cm apart. Tables 5 and 6 list the rail and foundation properties. Calculated track mobility is shown in lateral and vertical directions in Fig. 12.

Table 3 Wheel material properties Monk-Steel and Thompson (2003)

Parameter	Symbol	Unit	Value
Elastic modulus	E	GPa	200
Density	ρ	Kg/m3	7850
Poisson's ratio	ν	---	0.3

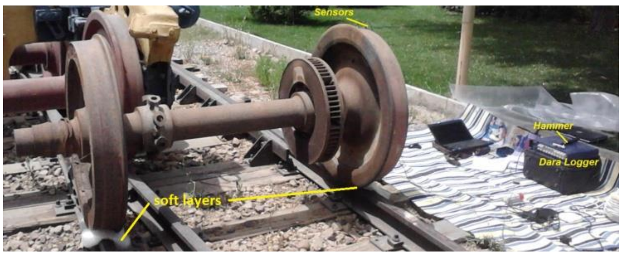

Fig. 10 Modal test setup

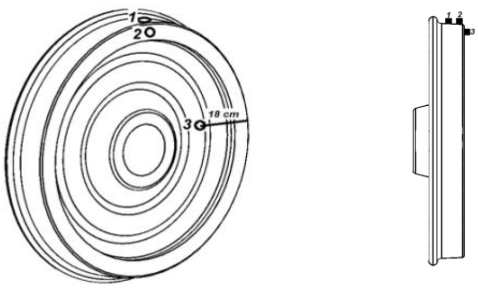

(a) test 1 (b) test 2

Fig. 11 Sensors configuration

Table 5 UIC 60 rail properties (Vincent and Thompson 1995)

Parameter	**Symbol**	**Unit**	**Value**
Elastic modulus	E	GPa	210
Density	ρ	Kg/m3	7850
Poisson's ratio	ν	---	0.3

Table 6 Track modeling parameters (Vincent and Thompson 1995), 1) Lateral, 2) Vertical

	C_b (KN.s/m)	**K_b (MN/m)**	**M_s (Kg)**	**C_{pr} (N.m.s)**	**K_{pr} (KN.m)**	**C_p (KN.s/m)**	**K_p (MN/m)**
1	48	80	162	163.5	654	12.5	50
2	50	50	162	-----	-----	87.5	350

5.3 Piezoelectric properties

Piezoelectric stack actuator is applied for inducing dithering in rail. Its properties and dimensions are listed in Table 7.

Properties for the employed piezoelectric patches in the wheel dithering are represented in Table 9 according to data sheet of a manufacturer. Dimensions of the piezoelectric patches are listed in Table 8.

Table 7 Piezoelectric stack properties PPA Datasheet & User Manual (2017)

Parameter	**Symbol**	**Unit**	**Value**
Longitudinal stiffness		kN/m	54000
Compliance module	S_{33}	m2/N	$19*10^{-12}$
Piezoelectric constant	d_{33}	m/V	$500*10^{-12}$
Density	ρ	Kg/m3	7800
Length	L	mm	244
Diameter	d	mm	25
Maximum elongation		mm	3
Allowable Voltage range		V	0-100

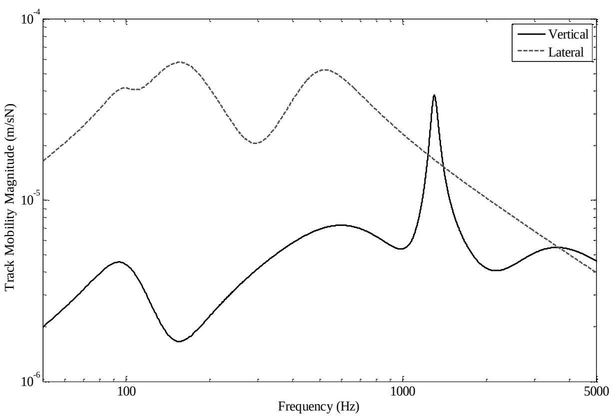

Fig. 12 Track mobility

Table 8 Piezoelectric patch dimension

Parameter	**Symbol**	**Value**	
Thickness	t_p	0.02 m	
Length	L_p	0.163 m	
Width	w_{pf}	front	0.058 m
	w_{pb}	back	0.04 m

Table 9 Piezoelectric patch properties PPA Datasheet & User Manual (2017)

Parameter	**Symbol**	**Unit**	**Value**
Relative permittivity	ε_{33}^{T}	---	1700
Piezoelectric constant	d_{31}	10e-12 m/V	190
Compliance matrix	S_{33}^{E}	10e-12 m^2/N	18.8
	S_{11}^{E}	10e-12 m^2/N	16.4
	S_{12}^{E}	10e-12 m^2/N	-5.74
	S_{13}^{E}	10e-12 m^2/N	-7.22
	S_{44}^{E}	10e-12 m^2/N	47.5
	S_{55}^{E}	10e-12 m^2/N	44.3
	S_{66}^{E}	10e-12 m^2/N	44.3

6. Model validation

Frequency content of the calculated wheel response and the squeal noise are shown in Figs. 13 and 14 respectively. In both figures the main peak occurs in the mode (2, 0) with the natural frequency of 365 Hz.

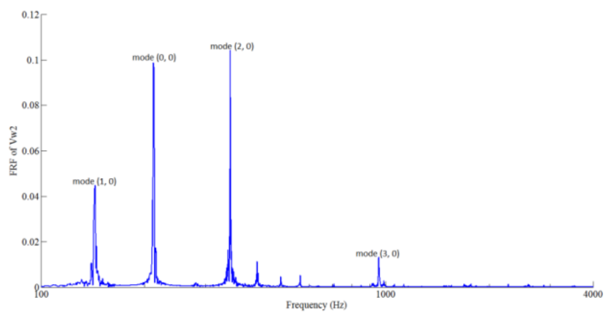

Fig. 13 FRF of lateral velocity of wheel

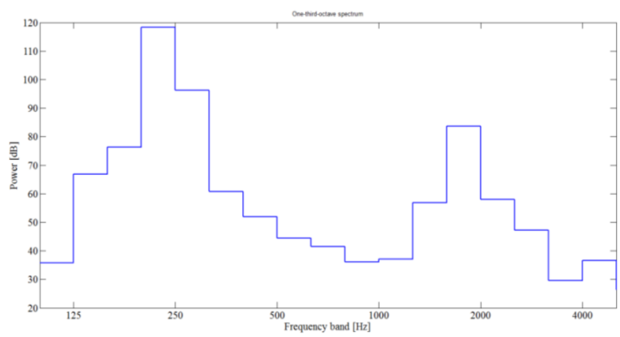

Fig. 14 Calculated wheel squeal noise

It is seen that the squealing happens and its noise level and frequency is quite close to the measurement results in the field test for a freight train.

7. Results

The results after applying dither signal to the wheel is presented and analyzed in this section. According to the wheel modal analysis, frequencies above 10 kHz might be selected. Fig. 15 shows the efficiency of the wheel dither control system on the squeal noise suppression. The maximum sound pressure level is decreased more than 35 dB. However, the induced dither signal causes an increase in the SPL in the frequency range higher than 3000 Hz. It is also seen that changes in voltage does not influence the dither control effect. As seen in Fig. 16, increasing the frequency of the applied voltage decreases the control efficiency. The best suppression performance can be achieved by taking the voltage amplitude equal to 10 V and its frequency to 10 kHz. Figs. 17 and 18 show the effect of dither control on the wheel responses.

Figs. 19 and 20 explain how wheel dithering causes suppression of squealing noise. As can be seen in Fig. 19, wheel dithering changes shape of lateral creepage from harmonic shape to random shape. As result range of lateral force on contact point variation has been decreased.

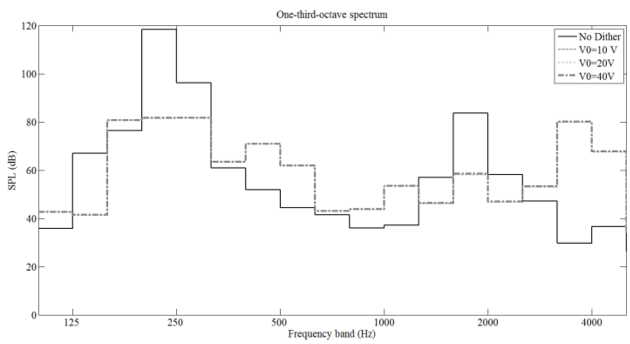

Fig. 15 Effect of the applied voltage amplitude on squeal noise reduction in wheel dither control ($\omega_0 = 10000 Hz$)

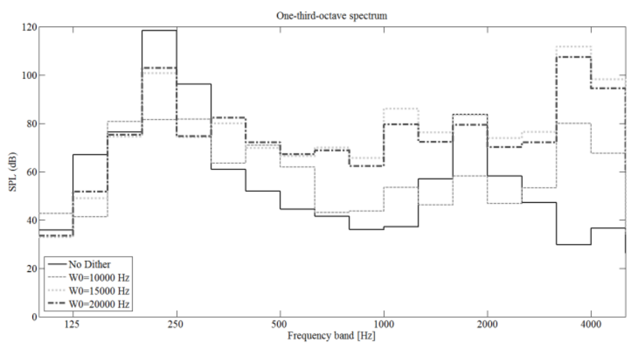

Fig. 16 Effect of the applied voltage frequency on the squeal noise reduction in wheel dither control ($V_0 = 10V$)

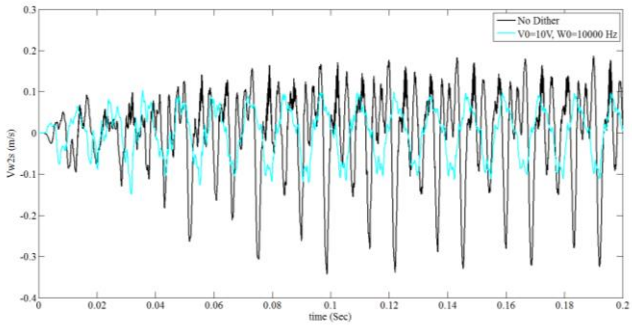

Fig. 17 Effect of the wheel dither control on lateral wheel velocity ($\omega_0 = 10000 Hz, V_0 = 10V$)

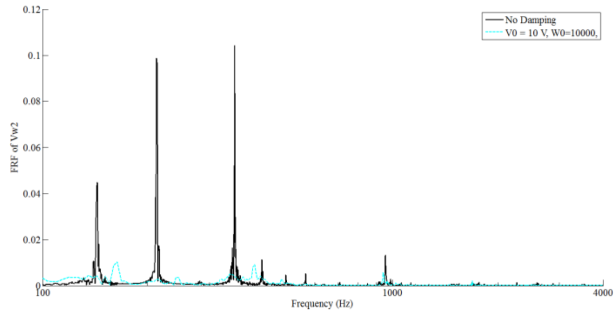

Fig. 18 Effect of the wheel dither control on the FRF of lateral wheel velocity ($\omega_0 = 10000 Hz, V_0 = 10V$)

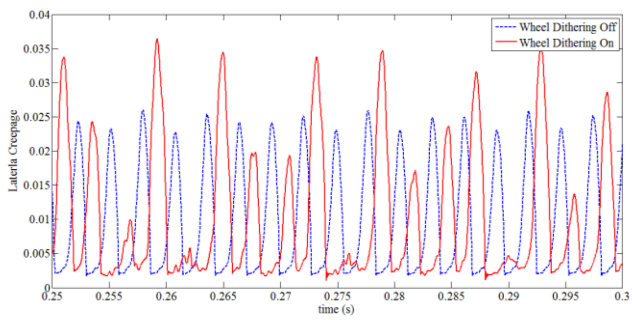

Fig. 19 Effect of the wheel dithering control on lateral creepage

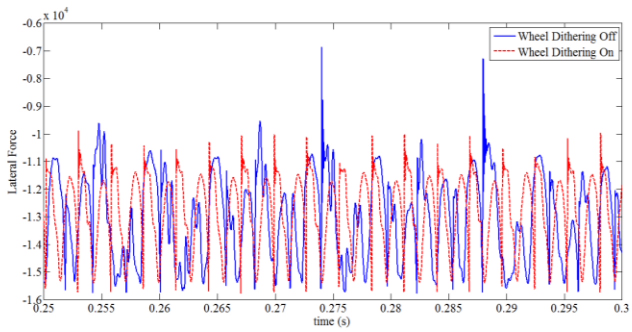

Fig. 20 Effect of the wheel dithering control on lateral force on contact point

Results when the dither control is applied to the rail are presented and discussed in this section. It is seen in Fig. 21 that the maximum squealing SPL is reduced to 85 dB from 118 dB. This reduction is in the frequency range lower than 700 Hz. Also this figure shows improving dither control effect by increasing the applied voltage. According to Fig. 22, relation between the applied voltage frequency and the squeal noise reduction is not linear. Effect of the rail dither control on the wheel responses in the time and frequency domain are shown in Figs. 23and 24.

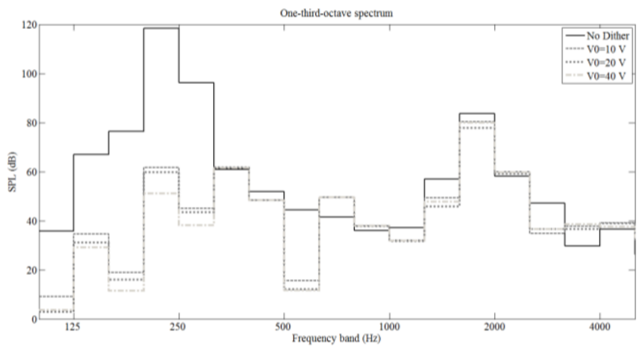

Fig. 21 Effect of applied voltage's amplitude on squeal noise reduction of rail dither control ($\omega_0 = 10000Hz$)

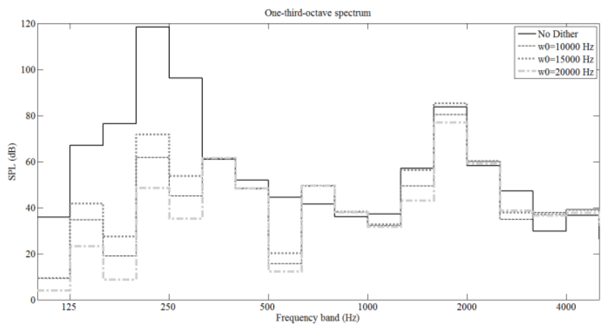

Fig. 22 Effect of applied voltage's frequency on squeal noise reduction of rail dither control ($V_0 = 10V$)

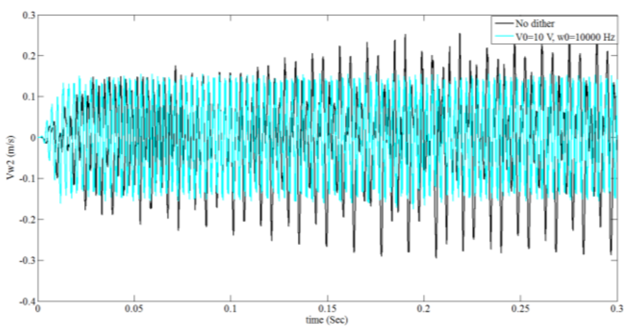

Fig. 23 Effect of rail dither control on lateral wheel velocity ($\omega_0 = 10000Hz$,$V_0 = 10V$)

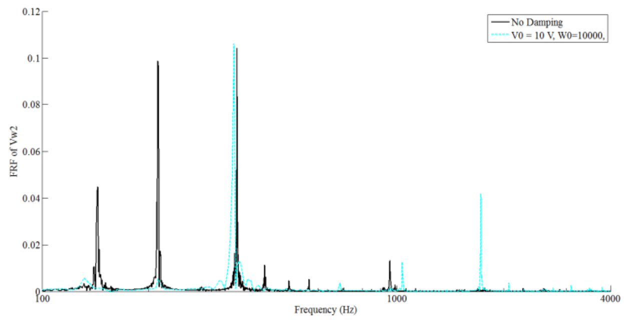

Fig. 24 Effect of wheel dither control on FRF of lateral wheel velocity ($\omega_0 = 10000Hz$,$V_0 = 10V$)

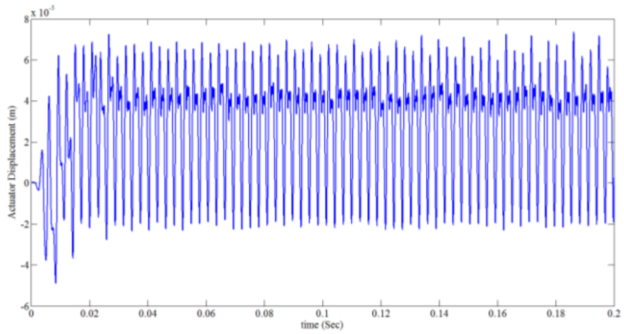

Fig. 25 Elongation of the piezoelectric stack actuator

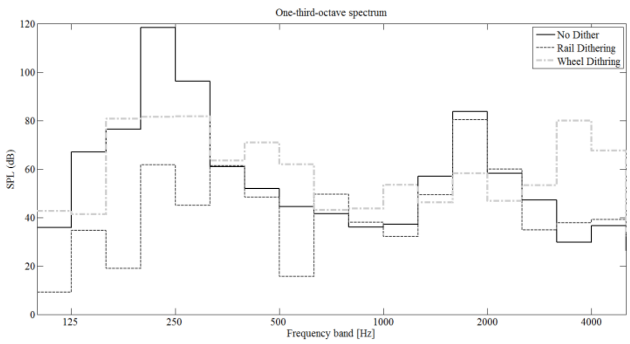

Fig. 26 Comparison between the wheel and rail dither control performance

Elongation of the piezoelectric actuators is limited as presented in Table 8. This limiting threshold should be checked. According to Fig. 25, maximum elongation is lower than the allowable limit. Performances of the two designs in squealing mitigation are compared in Fig. 26. It is seen that the rail dither control has better performance over almost all the frequencies. Besides this advantage, it must be noted that applying dither signal on the rail is much easier, cheaper and more feasible.

8. Conclusions

A comprehensive model for the wheel squealing simulation was developed in this paper. The model was validated on different levels and in total by comparing the results with field test data. As the main objective of this paper, the capability of a new approach in mitigation of squealing in sharp curves was investigated. Application of a dithering control to the wheel and rail was studied. As a first design, piezoelectric patches were attached to the appropriate locations on the wheel surface. It was found that dithering can reduce the noise level up to 35 dB in squealing frequency. Although this design may increase the noise level in higher frequencies but in total it can cancel the squalling and reduce the total noise level up to 10 dB. It was shown that the excessive control effort does not have remarkable effect on the performance while the dithering frequency slightly decreases the squealing noise but remarkably enhances the sound level in higher frequencies. Although applying this kind of semi-active control system to the wheel is somehow complicated but compared to other wheel-based solutions, it is independent of the wheel type. Toward a more feasible and practical design, dithering was applied to the rail. Economically and practically, this design is more appropriate, but we had to evaluate its performance. A stack type piezoelectric was used as dithering actuator in this second methodology. It was found that the second design has superior performance. It can not only cancel the squealing but also it is able to perform well in higher frequency range. It was also checked to guarantee that the system works within the threshold of piezoelectric saturation limit. Through a parametric study, it was shown that the actuator voltage is effectual this time and the dithering frequency influenced the performance more in the vicinity of the squealing frequency rather than in high frequency range.

References

Anderson, D., Wheatley, N., Fogarty, B., Jiang, J., Howie, A. and Potter, W. (2008), "Mitigation of curve squeal noise in Queensland, New South Wales and South Australia", *Proceedings of the Conference on Railway Engineering*, Australia, Perth, September.

Brunel, J.F., Dufrénoy, P. and Demilly, F. (2004), "Modelling of squeal noise attenuation of ring damped wheels", *Appl. Acoust*., **65**(5), 457-471.

Brunel, J.F., Dufrénoy, P., Charley, J. and Demilly, F. (2010), "Analysis of the attenuation of railway squeal noise by preloaded rings inserted in wheels", *J. Acoust. Soc. Am*., **127**(3), 1300-1306.

Curley, D., Anderson, D.C., Jiang, J. and Hanson, D. (2015), "Field trials of gauge face lubrication and top-of-rail friction modification for curve noise mitigation", Noise and Vibration Mitigation for Rail Transportation Systems, Germany, Heidelberg.

Garg, N. and Sharma, O. (2010), "Noise emissions of transit trains at curvature due to track lubrication", *Indian J. Pure Appl. Phys*., **48**(2010), 881-885.

Glocker, C., Cataldi-Spinola, E. and Leine, R.I. (2009), "Curve squealing of trains: Measurement, modelling and simulation", *J. Sound Vib*., **324**(1-2), 365-386.

Hanson, D., Jiang, J., Dowdell, B. and Dwight, R. (2014), "Curve squeal: causes, treatments and resultsn", *Proceedings of the 43rd International Congress on Noise Control Engineering*, Australia, Melbourne, October.

Hiensch, M., Dirks, B., Horst, J. and van der Stelt, J. (2007), "Rail head optimisation to reach a sustainable solution preventing Railway Squeal Noise", INTER-NOISE and NOISE-CON Congress and Conference Proceedings, Turkey, Istanbul, August.

Huang, Z.Y., Thompson, D.J. and Jones, C.J.C. (2007), "Squeal prediction for a bogied vehicle in a curve", Noise and Vibration Mitigation for Rail Transportation Systems, Germany, Berlin,September.

Jiang, S., Meehan, P.A., Thompson, D.J., and Jones, C.J.C. (2013), "Railway rolling noise prediction: field validation and sensitivity analysis", *Int. J. Rail Transport*., **1**(1-2), 109-127.

Jones, C.J.C. and Thompson, D.J. (2000), "Rolling noise generated by railway wheels with visco-elastic layers", *J. Sound Vib*., **231**(3), 779-790.

Kalker, J.J. (1991), "Wheel–rail rolling contact theory", Wear, 140, 243-266.

Knothe, K. and Wu, Y. (1998), "Receptance behaviour of railway track and subgrade", *Arch. Appl. Mech*., **68**(7-8), 457-470.

Kouroussis, G., Connolly, D.P. and Verlinden, O. (2014), "Railway-induced ground vibrations–a review of vehicle effects", *Int. J. Rail Transport*., **2**(2), 69-110.

Li, S.Q., Li, J., Mo, Y.P., Zhao, R. and Sun, Z.Y. (2014), "DOB-based piezoelectric vibration control for stiffened plate considering accelerometer measurement noise", *Smart Struct. Syst.*, **14**(3), 231-250.

Lin, B.C., Chang, S.C., Hu, J.F. and Lue, Y.F. (2015), "Controlling chaos for automotive disc brake squeal suppression", *J. Mech. Sci. Technol*., **29**(6), 2313-2322.

Liu, X. and Meehan, P.A. (2015), "Wheel squeal noise: A simplified model to simulate the effect of rolling speed and angle of attack", *J. Sound Vib*., **338**, 184-198.

Marjani, S.R. and Younesian, D. (2017), "Suppression of train wheel squeal noise by shunted piezoelectric elements", *Int. J. Struct. Stab. Dynam*., **17**(2), 1750027.

Meehan, P.A., Bellette, P.A., Jones, C. and Anderson, D. (2010), "Probabilistic prediction of wheel squeal under field humidity variationn", *Proceedings of the 20th International Congress on Acoustics*, Australia, Sydney, August.

Merideno, I., Nieto, J., Gil-Negrete, N., Landaberea, A. and Iartza, J. (2014), "Constrained layer damper modelling and performance evaluation for eliminating squeal noise in trams", *Shock Vib*., **2014**, 473720.

Monk-Steel, A.D. and Thompson, D.J., (2003), "Models for railways curve squeal noise", *Proceeding of the 8th International Conference on Recent Advances in Structural Dynamics*, England, Southampton, July.

Müller, B. and Oertli, J. (2006), "Combating curve squeal: monitoring existing applications", *J. Sound Vib*., **293**(3-5), 728-734.

Pieringer, A. (2014), "A numerical investigation of curve squeal in the case of constant wheel/rail friction", *J. Sound Vib*., **333**(18), 4295-4313.

Piezo Protection Advantage (PPA) Datasheet & User Manual (2017), Mide, Medford, USA. https://www.mide.com/collections/piezoelectric-products.

Ranjbar, M., Hardtke, H.J., Fritze, D. and Marburg, S. (2010), "Finding the best design within limited time: A comparative case study on methods for optimization in structural acoustics", *J. Comput. Acoust*., **18**(2), 149-164.

Ranjbar, M., Marburg, S. and Hardtke, H.J. (2012), "Structural-acoustic optimization of a rectangular plate: A Tabu search approach", *Finite Elem. Anal. Des*., **50**, 142-146.

Ranjbar, M., Marburg, S. and Hardtke, H.J. (2012), "A new hybrid design of experiments approach for optimization in structural acoustics applications", *Appl. Mech. Mater.*, **110**, 5015-5020.

Ranjbar, M. and Tadayon, A. (2017), "Vibration snalysis of multi degree of freedom self-excited systems", *J. Robot. Mechatron. Syst.*, **2**(1), 1-8.

Rusli, M., Bur, M. and Son, L. (2015), “Dynamic vibration absorber for squeal noise suppression in simple model structures”, *Int. J. Struct. Stab. Dynam*., **15**(5), 1450078.

Sadeghi, J., Khajehdezfuly, A., Esmaeili, M. and Poorveis, D. (2016), “An efficient algorithm for nonlinear analysis of vehicle/track interaction problems”, *Int. J. Struct. Stab. Dynam*., **16**(8), 1550040.

Shakeri, R. and Younesian, D. (2016), “Broad-band noise mitigation in vibrating annular plates by dynamic absorbers”, *Int. J. Struct. Stab. Dynam*., **16**(6), 1550014.

Soeta, Y. and Shimokura, R. (2013), “Survey of interior noise characteristics in various types of trains”, *Appl. Acoust*., **74**(10), 1160-1166.

Squicciarini, G., Usberti, S., Thompson, D.J., Corradi, R. and Barbera, A. (2015), “Curve squeal in the presence of two wheel/rail contact points”, Proceedings Noise and Vibration Mitigation for Rail Transportation Systems, Germany, Heidelberg.

Stefanelli, R., Dual, J. and Cataldi-Spinola, E. (2006). “Acoustic modelling of railway wheels and acoustic measurements to determine involved eigenmodes in the curve squealing phenomenon”, *Vehicle Syst. Dyn*., **44**(1), 286-295.

Teoh, C.Y. and MohdRipin, Z. (2017), “Dither effect on drum brake squeal”, *J. Vib. Control*, **23**(7), 1057-1072.

Thomsen, J.J. (1999), “Using fast vibrations to quench friction-induced oscillations”, *J. Sound Vib*., **228**(5), 1079-1102.

Vincent, N. and Thompson, D.J. (1995), “Track dynamic behaviour at high frequencies. Part 2: experimental results and comparisons with theory”, *Vehicle Syst. Dyn*., **24**(1), 100-114.

Vincent, N., Koch, J.R., Chollet, H. and Guerder, J.Y. (2006), “Curve squeal of urban rolling stock—Part 1: State of the art and field measurements”, *J. Sound Vib*., **293**(3-5), 691-700.

Volz, R. and Feldman, J. (2007), “Noise and Vibration Measurements of Curve Squel Noise Due to Trams on the Track”, *Proceedings of the 19th International Congress on Acoustics*, Spain, Madrid, September.

Younesian, D. and Kargarnovin, M.H. (2009), “Response of the beams on random Pasternak foundations subjected to harmonic moving loads”, *Mech. Sci. Technol.*, **23**(11), 3013-3023.

Younesian, D., Aleghafourian, M.H. and Esmailzadeh, E. (2015), “Vibration analysis of circular annular plates subjected to peripheral rotating transverse loads”, *J. Vib. Control*, **21**(7), 1443-1455.

Zenz, G., Berger, W., Gerstmayr, J., Nader, M. and Krommer, M. (2013), “Design of piezoelectric transducer arrays for passive and active modal control of thin plates”, *Smart Struct. Syst*., **12**(5), 547-577.

HJ